Surv Geophys (2018) 39:729–751
https://doi.org/10.1007/s10712-018-9465-3

Quantifying Modern Recharge and Depletion Rates of the Nubian Aquifer in Egypt

Mohamed Ahmed[1,2] · Karem Abdelmohsen[1]

Received: 4 April 2017 / Accepted: 9 February 2018 / Published online: 20 February 2018

Abstract Egypt is currently seeking additional freshwater resources to support national reclamation projects based mainly on the Nubian aquifer groundwater resources. In this study, temporal (April 2002 to June 2016) Gravity Recovery and Climate Experiment (GRACE)-derived terrestrial water storage (TWS_{GRACE}) along with other relevant datasets was used to monitor and quantify modern recharge and depletion rates of the Nubian aquifer in Egypt (NAE) and investigate the interaction of the NAE with artificial lakes. Results indicate: (1) the NAE is receiving a total recharge of 20.27 ± 1.95 km^3 during 4/2002−2/2006 and 4/2008–6/2016 periods, (2) recharge events occur only under excessive precipitation conditions over the Nubian recharge domains and/or under a significant rise in Lake Nasser levels, (3) the NAE is witnessing a groundwater depletion of $-$ 13.45 $\pm$ 0.82 km^3/year during 3/2006–3/2008 period, (4) the observed groundwater depletion is largely related to exceptional drought conditions and/or normal baseflow recession, and (5) a conjunctive surface water and groundwater management plan needs to be adapted to develop sustainable water resources management in the NAE. Findings demonstrate the use of global monthly TWS_{GRACE} solutions as a practical, informative, and cost-effective approach for monitoring aquifer systems across the globe.

Keywords GRACE · Terrestrial water storage · Groundwater storage · Recharge · Depletion · Nubian aquifer in Egypt

Abbreviations

AAR	Average annual rainfall
AFWA	Air Force Weather Agency
AVHRR	Advanced Very High-Resolution Radiometer

✉ Mohamed Ahmed
mohamed.ahmed@wmich.edu

1 Department of Geosciences, Western Michigan University, 1903 West Michigan Avenue, Kalamazoo, MI 49008, USA

2 Department of Geology, Faculty of Science, Suez Canal University, Ismailia 41522, Egypt

CLM	Community land model
CMAP	Climate Prediction Center Merged Analysis of Precipitation
CRI	Coastline resolution improvement
DEM	Digital elevation model
DLR	German Aerospace Center
ETM	Enhanced Thematic Mapper
GDAS	Global Data Assimilation System
GIA	Glacial isostatic adjustment
GIS	Geographic information system
GLAS	Geoscience Laser Altimeter System
GLDAS	Global Land Data Assimilation System
GOES	Geostationary Operational Environmental Satellite
GOHS	Equipe Géodésie, Océanographie & Hydrologie Spatiales
GPCC	Global Precipitation Climatology Centre
GPI	GOES Precipitation Index
GRACE	Gravity Recovery and Climate Experiment
GRLM	Global reservoir and lake monitoring
GWS	Groundwater storage
JPL	Jet Propulsion Laboratory
LEGOS	Laboratoire d'Etudes en Geodésie et Océanographie Spatiales
LSM	Land surface model
Mascons	Mass concentration
MODIS	MODerate-resolution Imaging Spectroradiometer
MSU	Microwave sounding unit
NAE	Nubian aquifer in Egypt
NASA	National Aeronautics and Space Administration
NCAR	National Centre for Atmospheric Research
NOAA	National Oceanic and Atmospheric Administration
OLR	Outgoing Longwave Radiation
OPI	OLR-based Precipitation Index
SMS	Soil moisture storage
SSM/I	Special Sensor Microwave/Imager
SWS	Surface water storage
TM	Thematic Mapper
TWS	Terrestrial water storage
USDA-FAS	U.S. Department of Agriculture's Foreign Agricultural Service
UT-CSR	University of Texas Center for Space Research
VIC	Variable infiltration capacity

1 Introduction

The understanding of the geologic and hydrologic settings of, and the controlling factors affecting, freshwater resources in Egypt is gaining increasing importance due to the challenges posed by natural and anthropogenic forcing factors. The natural factors might include, but are not limited to, changes in rainfall and/or temperature patterns, duration, and magnitude, whereas the anthropogenic factors could include population growth, overexploitation, and pollution. Given the Egyptian hyper-arid climate, Egypt is currently receiving very little annual rainfall, distributed as 50, 20, and 5 mm over the Sinai Peninsula, Eastern Desert, and Western Desert, respectively (Ahmed et al. 2013; Mohamed et al. 2015). These minimal rainfall amounts and the relatively higher air temperature (~ 30 °C) are extremely vulnerable to climate change. Recent climate change studies over Africa indicated a tendency toward higher extremes, where the arid or semiarid areas will becoming increasingly dry and the wetter areas will witness intensified precipitation and flooding (Vörösmarty et al. 2000; Hulme et al. 2001).

Egypt's total population is on rise; it increased from 22 million in 1950 to 94 million in 2016 and is expected to continue for decades to come. The majority (95%) of the Egyptian population lives in the Nile River valley and Nile Delta (~ 10% of Egypt's area), whereas Egypt's deserts remain largely uninhabited, causing enormous pressures on the Nile River surface water resources. Given the fact that the Nile basin is largely extended over varying topographic and climatic regimes, it represents one of the most vulnerable river systems across the world. Recent studies have shown that Nile basin countries are expected to experience a water stress that will be manifested as changes in precipitation patterns, amounts, frequencies, and distributions along with changes in temperature, changes in river flow, and the occurrence of associated floods and drought events (e.g., Swain 2011). Egypt currently uses its total annual allocation (55 km^3/year) of Nile River waters coming mainly (~ 85%) from the Blue Nile. In addition, some of the Nile River source countries declared that they will no longer abide by the treaty that regulated the distribution of the Nile River water. For example, Ethiopia just launched a major project to construct the Grand Ethiopian Renaissance Dam which will deprive Egypt of considerable portions of its Blue Nile water for several years. Recent studies (e.g., Sultan et al. 2014b) have shown that if the Grand Ethiopian Renaissance Dam reservoir (capacity: 70 km^3) is to be filled in seven years, Egypt will lose, for each of the seven years following dam completion, a minimum of 15 km^3 of its annual allocation to reservoir filling (10 km^3), evaporation (3.5 km^3), and infiltration (1.5 km^3).

Egypt is seeking additional freshwater resources to overcome some of the aforementioned challenges and to pursue its plans for modernization and development. Currently, Egypt is planning to utilize more of its groundwater resources, at the expense of Nile River water, to support national reclamation projects; a minimum of 1.5×10^6 acres will be reclaimed during the coming five years. According to the hydrogeological map of Egypt (RIGW/IWACO 1988), Egyptian aquifer systems (Fig. 1) include (1) the Nile aquifer that occupies the Nile flood plain and desert fringes (Late Tertiary to Quaternary); (2) the Moghra aquifer which occupies the western edge of the Delta (Lower Miocene); (3) the coastal aquifer that is distributed over northern and eastern coasts (Late Tertiary to Quaternary); (4) the carbonate aquifer in the north and middle parts of the Western Desert (Upper Cretaceous to Eocene); (5) the fractured basement aquifer in the Eastern Desert and Sinai Peninsula (Precambrian); and (6) the Nubian aquifer covering the Western Desert, western parts of the Eastern Desert, and the middle parts of Sinai Peninsula (Cambrian to Upper Cretaceous). The majority of current Egyptian reclamation projects depend mainly on Nubian aquifer water resources.

The Nubian aquifer (area: 2×10^6 km^2; Fig. 1, inset a) represents a transboundary aquifer system shared by four countries: Egypt (38%), Libya (34%), Sudan (17%), and Chad (11%), where the majority of the aquifer's water resources are located in Egypt (41.5 vol%) and Libya (41.5 vol%), and less of it in Chad (12.8 vol%) and Sudan (9 vol%) (Thorweihe and Heinl 2002). The Nubian aquifer contains three major sub-basins: the Dakhla sub-basin in Egypt; the Kufra sub-basin in Libya, northeastern Chad, and northwestern Sudan; and the northern Sudan sub-basin in northern Sudan (Fig. 1, inset a). The Dakhla

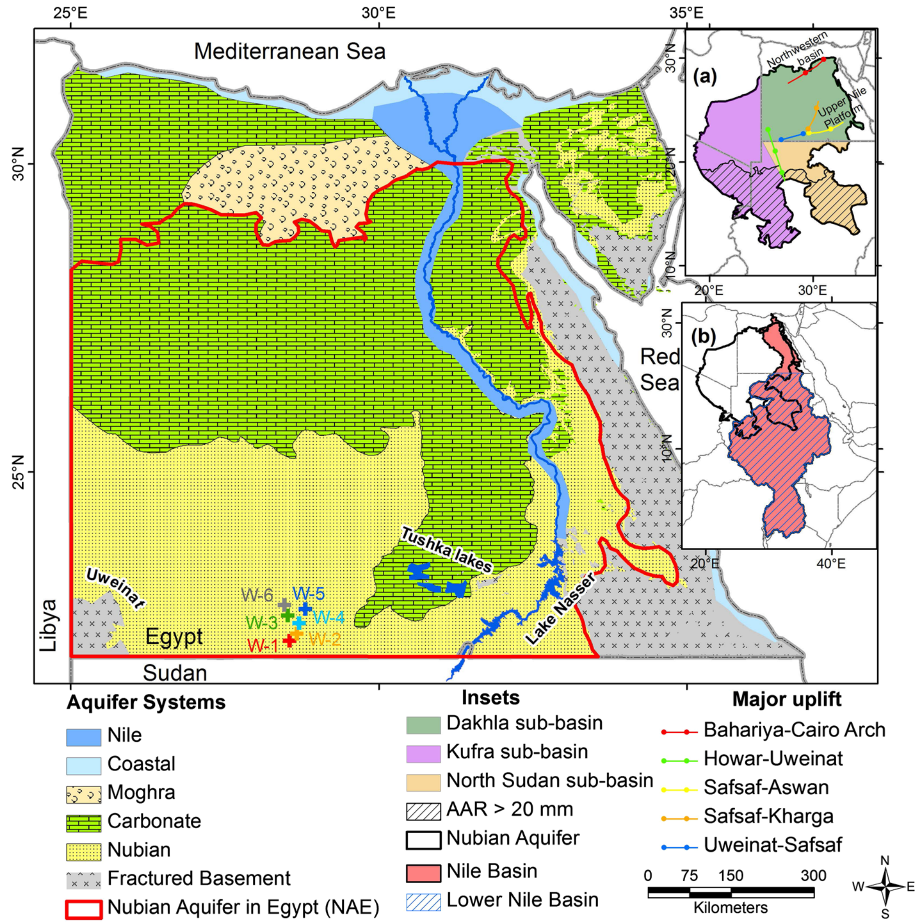

Fig. 1 Hydrogeologic map showing the spatial distribution of the major aquifer systems in Egypt (RIGW/IWACO 1988). Also shown are the spatial extension of the NAE (red polygon) and the spatial distribution of monitoring wells (colored crosses). Inset **a** The spatial extension of the Nubian aquifer sub-basins in Egypt, Libya, Chad, and Sudan as well as the major uplift. Also shown is the spatial extension of the Nubian recharge domains that extend over the aquifer outcrops and receive average annual rainfall (AAR) greater than 20 mm (hatched area). Inset **b** The spatial extension of the entire Nile basin along with the lower Nile basin (hatched area)

sub-basin in Egypt extends over two minor rift-related sub-basins: the Northwestern basin and the Upper Nile Platform (Fig. 1, inset a). In this study, the Dakhla sub-basin in Egypt was called the Nubian aquifer in Egypt (NAE). Given the fact that the health of the NAE affects the success of the Egyptian reclamation projects as well as the livelihood of many people, the ability to routinely observe the water resources of the NAE and make those observations publicly available to the decision makers is inevitable. In situ observations (e.g., groundwater levels) of the NAE suffer from delay, gaps, discontinuity, inconsistency, and poor quality. Moreover, these observations are sparse and do not adequately represent the entire aquifer (NAE area: 0.66×10^6 km^2) averaged estimates. Satellite remote sensing observations offer an alternative and/or complement to local in situ measurements and could be used to monitor the aquifer health and longevity. Most of these observations are globally distributed, free and publicly available, and temporally and spatially homogeneous.

The deployment of the Gravity Recovery and Climate Experiment (GRACE) mission and the collection of global temporal gravity fields over the past 15 years provide significant practical strategies to routinely observe and monitor the water resources of the NAE. The GRACE mission, sponsored jointly by the National Aeronautics and Space Administration (NASA) and the German Aerospace Center (DLR), is designed to map the temporal variations in Earth's global gravity field on a monthly basis with unprecedented accuracy (Tapley et al. 2004a, b). The GRACE-derived variabilities in Earth's gravity field can be used to make global estimates of the spatiotemporal variations in the total vertically integrated components (e.g., surface water, groundwater, soil moisture and permafrost, snow and ice, wet biomass) of terrestrial water storage (TWS) (Wahr et al. 1998).

The GRACE-derived TWS (TWS_{GRACE}) data enabled the scientific community to address previously unresolvable hydrogeological questions (e.g., Ahmed et al. 2011, 2014b, 2016; Wouters et al. 2014; Fallatah et al. 2017). GRACE data have been extensively used to quantify aquifers' recharge and depletion rates (e.g., Tiwari et al. 2009; Lenk 2013; Voss et al. 2013; Feng et al. 2013; Gonçalvès et al. 2013; Joodaki et al. 2014; Sultan et al. 2014a; Wouters et al. 2014; Castle et al. 2014; Döll et al. 2014; Al-Zyoud et al. 2015; Huang et al. 2015, 2016; Li and Rodell 2015; Chinnasamy and Agoramoorthy 2015; Chinnasamy et al. 2015; Ahmed et al. 2016; Huo et al. 2016; Jiang et al. 2016; Lakshmi, 2016; Long et al. 2016; Mohamed et al. 2016; Castellazzi et al. 2016; Veit and Conrad 2016; Wada et al. 2016; Yosri et al. 2016; Chinnasamy and Sunde 2016). Recent studies utilizing TWS_{GRACE} data have shown that the NAE is witnessing an overall groundwater depletion. The reported groundwater depletion rates of the NAE varied with the examined period as well as the data sources. For example, groundwater depletion rates of 2.31 ± 1.00, 2.04 ± 0.99, 4.44 ± 0.42, and 2.58 ± 0.73 km^3 were reported during the periods of April 2002 to November 2010, January 2003 to September 2012, January 2003 to December 2012, and April 2002 to December 2013, respectively (Sultan et al. 2013, 2014b; Ahmed et al. 2014a, 2015; Mohamed et al. 2015). Mohamed et al. (2016) have shown that the Nubian aquifer, from January 2003 to December 2012, is receiving an average annual recharge of 0.78 ± 0.49 and 1.44 ± 0.42 km^3/year over the recharge domains in Sudan and Chad, respectively. By comparison, the Nubian aquifer in Libya and Egypt is witnessing a groundwater depletion of 0.48 ± 0.32 and 4.44 ± 0.42 km^3/year, respectively. None of these studies has reported and/or quantified the amounts of natural recharge that the NAE is witnessing. Moreover, the recharge/discharge interaction of the NAE with artificial lakes, such as Lake Nasser and the Tushka Lakes, has not been clearly explained in many of these studies (Soltan et al. 2005; Sefelnasr 2007; Sefelnasr et al. 2015).

In this study, temporal (April 2002 to June 2016) TWS_{GRACE} data along with the outputs of land surface models (LSMs) were used to provide improved estimates of recharge and depletion rates of the NAE. This study extends the previous investigations by (1) utilizing enhanced state-of-the-art TWS_{GRACE} solutions, the global mass concentration solutions (mascons); (2) utilizing outputs from several LSMs; four versions of the Global Land Data Assimilation System (GLDAS) to isolate the GRACE-derived groundwater storage (GWS); (3) broadening the time interval by four years; and (4) investigating the interaction of the NAE with artificial lakes, such as Lake Nasser and the Tushka Lakes.

2 Data and Methods

In this section, a brief description of the GRACE, surface water, soil moisture, and rainfall datasets used in this study is provided. The procedures used to extract TWS_{GRACE}, surface water storage (SWS), soil moisture storage (SMS) anomalies, and AAR are also presented in this section. All of the datasets used in this exercise are monthly and were acquired throughout the time period of April 2002 to June 2016.

2.1 GRACE-Derived TWS (TWS_{GRACE}) Data

Three sources of GRACE data have been utilized in this study: spherical harmonics and mascon products of the University of Texas Center for Space Research (UT-CSR) and mascon solutions from the Jet Propulsion Laboratory (JPL). It is worth mentioning that, compared to the spherical harmonics fields, the mascon solutions provide higher signal-to-noise ratio, higher spatial resolution, and reduced error and do not require spectral (e.g., destriping) and spatial (e.g., smoothing) filtering or any empirical scaling techniques (Luthcke et al. 2013; Watkins et al. 2015; Save et al. 2016; Wiese et al. 2016; Scanlon et al. 2016). However, rescaling spherical harmonic solutions significantly increases the agreement with mascon solutions (Watkins et al. 2015; Scanlon et al. 2016).

The spherical harmonics of the UT-CSR GRACE solution (Level 2; Release 05; degree/order: 60; available at: ftp://podaac.jpl.nasa.gov/allData/grace/L2/CSR/RL05) were used in this study. The GRACE-derived *C20* and degree-1 coefficients were replaced with those estimated by Cheng et al. (2011) and Swenson et al. (2008), respectively. The glacial isostatic adjustment (GIA) correction was applied using the GIA model developed by A et al. (2013). The temporal mean (April 2002 to June 2016) was removed from these solutions, and systematic and random errors were reduced by applying destriping and Gaussian (half-width: 200 km) filters, respectively (Wahr et al. 1998; Swenson and Wahr 2006). Following the procedures advanced by Wahr et al. (1998), the spherical harmonic coefficients were then converted to TWS_{GRACE} grids of equivalent water thickness.

The generated TWS_{GRACE} grids were then rescaled to minimize the attenuation in the amplitude of the TWS_{GRACE} time series due to the application of GRACE post-processing steps (e.g., Landerer and Swenson 2012; Long et al. 2015). The approach described in Velicogna and Wahr (2006) was adapted to scale TWS_{GRACE}. Two synthetic mass distributions were assumed across the NAE, converted into Stokes coefficients (up to degree 60), filtered using destriping and Gaussian (200 km) filters, and then reconverted to mass distributions. The ratio of the recalculated mass distribution to the original mass distribution is called the scaling factor. One of the selected synthetic mass distributions was chosen to represent the global TWS_{GRACE} trend results, while the other was set to be 1.0 inside the NEA spatial domain and 0.0 outside it. These synthetic mass distributions were selected to reflect a real picture of what the TWS_{GRACE} trends look like across the NAE spatial domain. The final scaling factor (1.90 $\pm$ 0.80) was selected as the average of the two scaling factors, generated by using the two different synthetic mass distributions, whereas the difference was used to quantify errors associated with that scaling factor. Raw TWS_{GRACE} estimates over the NAE were then multiplied by the generated scaling factor to calculate the scaled TWS_{GRACE} estimates.

The JPL mascon data (Release 05; version 2; 0.5° × 0.5° grid; available at: ftp://podaac.jpl.nasa.gov/allData/tellus/L3/mascon/RL05/JPL/) provide monthly gravity field variations for 4551 equal areas of 3° spherical caps. The coastline resolution improvement

(CRI) filtered data, utilized to determine the land and ocean fractions of mass inside every land/sea mascon, were used in this study (Watkins et al. 2015; Wiese et al. 2016). The UT-CSR mascon solutions (Release 05; version 1; 0.5° × 0.5° grid; available at: http://www.csr.utexas.edu/grace/RL05_mascons.html) approach uses the geodesic grid technique to model the surface of the Earth using equal area gridded representation of the Earth via 40,962 cells (40,950 hexagons + 12 pentagons) (Save et al. 2012, 2016). The size of each cell is about equatorial 1°, the number of cells along the equator is 320, the average area of each cell is 12,400 km^2, and the average distance between cell centers is 120 km. The UT-CSR mascon does not suffer from oversampling at the poles like an equiangular grid (Save et al. 2016).

The secular trend in $\mathrm{TWS_{GRACE}}$ data was extracted by simultaneously fitting a trend and seasonal (e.g., annual and semiannual) terms to each $\mathrm{TWS_{GRACE}}$ time series. The trend solutions are displayed in Fig. 2. Errors associated with monthly $\mathrm{TWS_{GRACE}}$ and calculated trend values were then estimated (Tiwari et al. 2009; Scanlon et al. 2016): (1) monthly $\mathrm{TWS_{GRACE}}$ time series were fitted using annual, semiannual, and trend terms and residuals ($R1$) were calculated; (2) $R1$ were smoothed using a 13-month moving average, a trend was removed, and the residuals ($R2$) were calculated; (3) the standard deviation of $R2$ represents the maximum uncertainty in monthly $\mathrm{TWS_{GRACE}}$ values; (4) Monte Carlo simulations (e.g., Hastings 1970; Vrugt et al. 2009) were performed by fitting trends and seasonal terms for many (n = 20,000) synthetic monthly datasets, each with values chosen from a population of Gaussian-distributed numbers having a standard deviation similar to that of the examined population; and (5) the standard deviation of the extracted synthetic trends was interpreted as the trend error for $\mathrm{TWS_{GRACE}}$. The generated trend data were then statistically analyzed by using parametric techniques (i.e., Student t test) to identify trends that are statistically significant at 95 and at 65% levels of confidence.

Given the fact that $\mathrm{TWS_{GRACE}}$ data have no vertical resolution, since GRACE cannot distinguish between anomalies resulting from different components of TWS (e.g., surface water, soil moisture, and groundwater), the contributions of SWS and SMS need to be quantified and removed from $\mathrm{TWS_{GRACE}}$ time series (Fig. 3) to calculate GWS according to the following equation:

$$\Delta\mathrm{GWS_{GRACE}} = \Delta\mathrm{TWS_{GRACE}} - \Delta\mathrm{SMS} - \Delta\mathrm{SWS}, \tag{1}$$

where ΔGWS, ΔSWS, and ΔSMS represent the change, with respect to the temporal (April 2002 to June 2016) mean, in groundwater, surface water, and soil moisture storage, respectively. Errors in GWS are then estimated by adding, in quadrature, errors associated with $\mathrm{TWS_{GRACE}}$, SWS, and SMS according to the following equation:

$$\sigma_{\mathrm{GWS_{GRACE}}} = \sqrt{(\sigma_{\mathrm{TWS_{GRACE}}})^2 + \left(\sigma_{\mathrm{SMS}}\right)^2 + \left(\sigma_{\mathrm{SWS}}\right)^2}, \tag{2}$$

where $\sigma_{\mathrm{TWS_{GRACE}}}$, σ_{SMS}, and σ_{SWS} represent errors in ΔTWS, ΔSWS, and ΔSMS, respectively.

2.2 SWS Data

Two main surface water reservoirs within the NAE were examined: Lake Nasser and the Tushka Lakes (Fig. 1). Both reservoirs are expected to affect $\mathrm{TWS_{GRACE}}$ and therefore GWS estimates over the NAE. Figure 4, for example, shows the GRACE average sensitivity kernel function over the Lake Nasser. The sensitivity kernel function is generated by

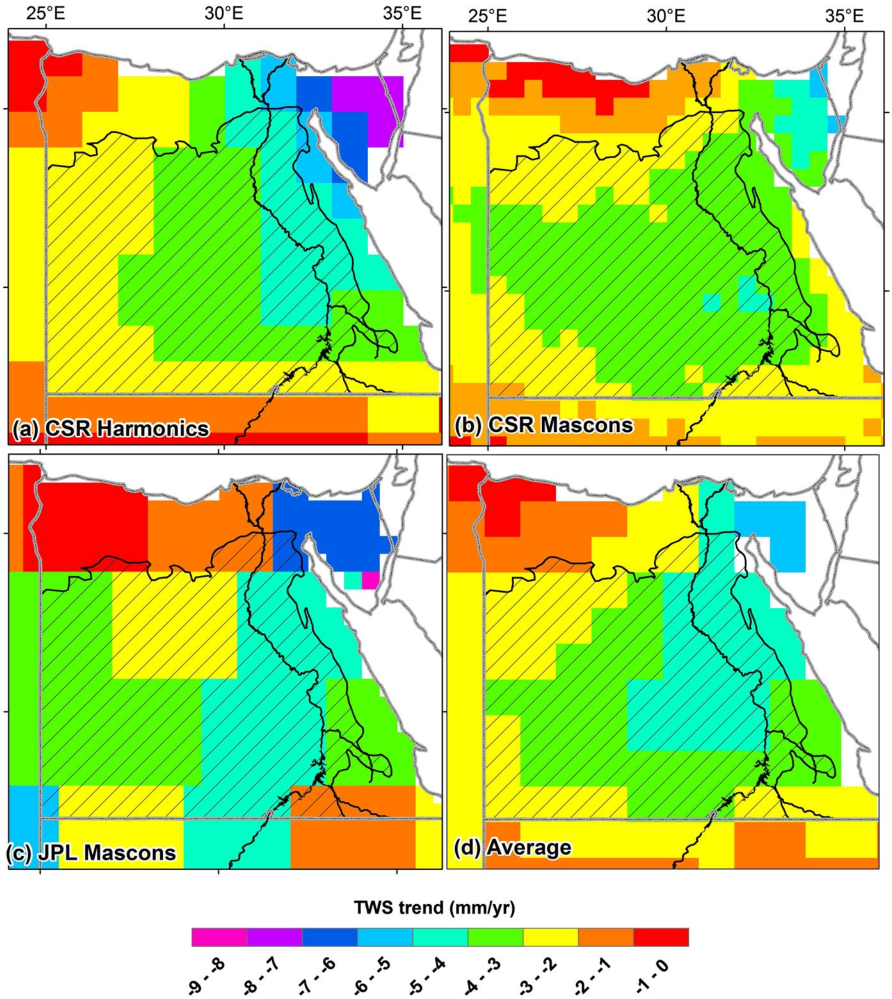

Fig. 2 Secular trend images of monthly (April 2002 to June 2016) TWS_{GRACE} estimates generated, from **a** UT-CSR spherical harmonics, **b** UT-CSR mascons, **c** JPL mascons, and **d** average solution over the NAE and surroundings. Also shown is the spatial extension of the NAE (hatched area)

converting 1 cm uniformly distributed Lake Nasser height into monthly Stokes coefficients up to degree 60.

The Lake Nasser surface levels time series was extracted from averaging two main surface water-level datasets: (1) the U.S. Department of Agriculture's Foreign Agricultural Service (USDA-FAS) global reservoir and lake monitoring database (GRLM; available at: https://www.pecad.fas.usda.gov/cropexplorer/global_reservoir/), and (2) the Hydroweb database at Laboratoire d'Etudes en Geophysique et Oceanographie Spatiales (LEGOS/GOHS; available at: http://www.legos.obs-mip.fr/fr/soa/hydrologie/hydroweb/) (Crétaux et al. 2011). The Lake Nasser monthly level anomalies were then generated, with respect to the temporal mean (April 2002 to June 2016), over the entire NAE (Fig. 5a). The accuracy of lake levels derived from these two databases has been estimated at 3–4 cm for the

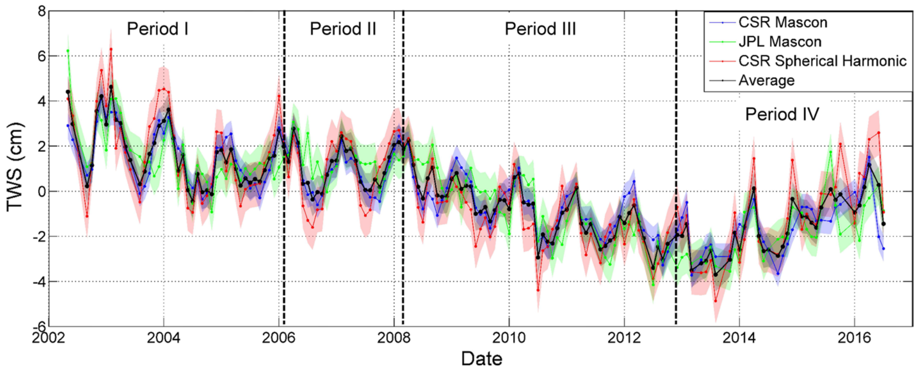

Fig. 3 Temporal variations in TWS_{GRACE} estimates, along with the associated uncertainties, extracted from the UT-CSR mascons (blue line), JPL mascons (green line), UT-CSR spherical harmonics (red line), and average (black line) solutions over the NAE

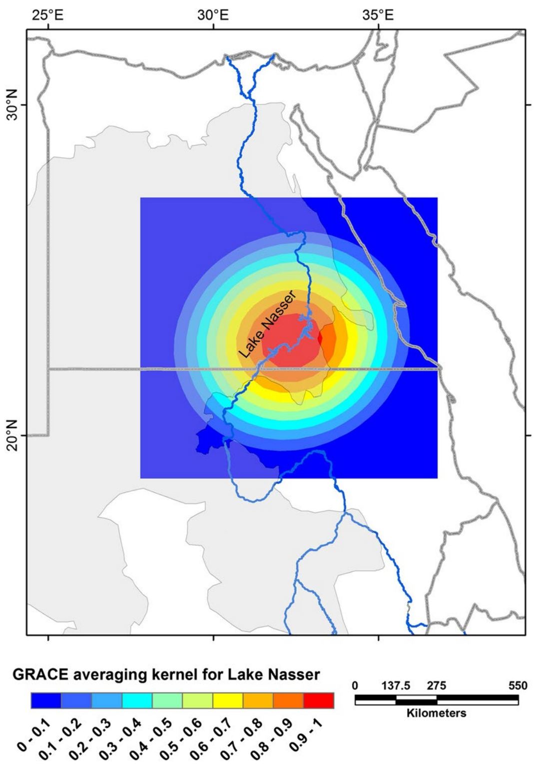

Fig. 4 GRACE unscaled dimensionless averaging sensitivity kernel function generated over the Lake Nasser area within the NAE

largest lakes (Birkett 1995; Shum et al. 2003; Swenson and Wahr 2009). In this study, the monthly errors in Lake Nasser level estimates were calculated as the standard deviation of sub-monthly water levels collected from Hydroweb and GRLM databases (e.g., Muala

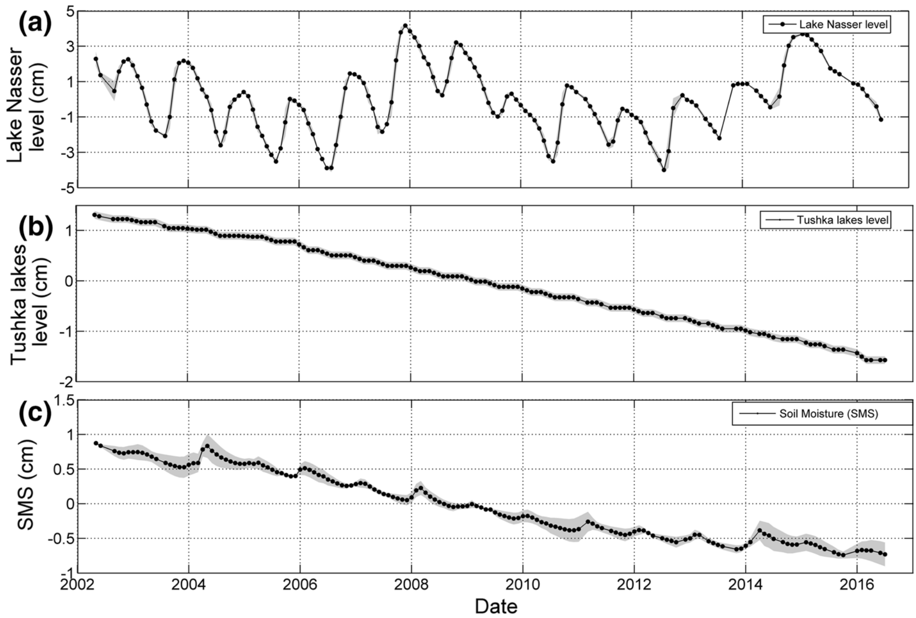

Fig. 5 Temporal variations, averaged over the NAE, in **a** Lake Nasser level anomalies, **b** Tushka Lakes level anomalies, and **c** SMS. Also shown are the uncertainty limits associated with each monthly value

et al. 2014). Trends in Lake Nasser levels and associated trend errors were estimated using the procedures described for TWS_{GRACE}.

The Tushka spillway was constructed in 1978 to protect the Aswan High Dam from cyclic flooding events. In 1990, Lake Nasser started to rise; it reached a height of 182 m and spilled over into the Tushka spillway in September 1998. This event resulted in the formation of the first Tushka Lake. In subsequent years, as water continued to flow through the spillway, five additional lakes were created (Fig. 1). Examination of temporal satellite images indicates a gradual decrease in areas and volumes of the Tushka Lakes. Over 80% of the loss is via evaporation given the low permeability of the variegated shale underlying much of these lakes (e.g., Sultan et al. 2013). In this study, the monthly volume, area, and water height decrease in the Tushka Lakes were quantified. Two Landsat images (paths: 176 and 175; row: 44; spatial resolution: 30 m; available at: https://earthexplorer.usgs.gov/) were mosaicked and used to quantify the temporal variations, in water covered areas, of the Tushka Lakes in a geographic information system (GIS) environment. Landsat 5 Thematic Mapper (TM) images, Landsat 7 Enhanced Thematic Mapper (ETM +) images, and Landsat 8 images were used for the 2002, 2003–2012, and 2013–2016 periods, respectively. The Tushka Lakes' volumes were calculated using the areas and water depth information. The water depth estimates were quantified using a digital elevation model (DEM; spatial resolution: 90 m), acquired prior to the formation of the Tushka Lakes, and validated using data extracted from topographic sheets (scale 1: 100,000). A 10% error estimate for the Tushka Lakes level time series was assumed (e.g., Castle et al. 2014). Moreover, the Tushka Lakes' volumes during the period from 2002 to 2010 were compared to, and validated against, volumes extracted using different remote sensing images [e.g., MODerate-resolution Imaging Spectroradiometer (MODIS) and Advanced Very High-Resolution Radiometer

(AVHRR) for area calculations and Geoscience Laser Altimeter System (GLAS) for water-level estimation] and techniques (e.g., Chipman and Lillesand 2007; Lillesand et al. 2015). The Tushka Lakes' monthly level anomalies were then generated with respect to the temporal mean (April 2002 to June 2016) and averaged over the entire NAE (Fig. 5b). Trends in the Tushka Lakes' levels and associated trend errors were estimated using the procedures described for TWS_{GRACE}.

2.3 SMS Data

Soil moisture data (Fig. 5c) were extracted from GLDAS model (version 1; available at: ftp://hydro1.sci.gsfc.nasa.gov) given that previous studies over Saharan Africa (Ahmed et al. 2016) have shown that GLDAS provides more reasonable estimates of soil moisture in arid areas when compared to estimates from other LSMs. GLDAS is a NASA-developed land surface modeling system which performs advanced simulations to quantify optimal fields of land surface states (e.g., soil moisture, snow, surface temperature) and fluxes (e.g., evapotranspiration, ground heat flux) using ground and satellite-based observations (Rodell et al. 2004). Soil and elevation data inputs are based on high-resolution globally distributed datasets. The Climate Prediction Center (CPC) Merged Analysis of Precipitation (CMAP) data represents the precipitation inputs, whereas the radiation inputs are generated from the observation based downward radiation products, derived using Air Force Weather Agency (AFWA) fields and procedures. Other meteorological forcing data are produced by the National Oceanic and Atmospheric Administration (NOAA) Global Data Assimilation System (GDAS) atmospheric analysis system (Rodell et al. 2004). The GLDAS model simulates soil moisture through four versions: variable infiltration capacity (VIC), community land model (CLM), Noah, and Mosaic (Koster and Suarez 1996; Liang et al. 1996; Koren et al. 1999; Dai et al. 2003; Rodell et al. 2004). The soil moisture time series over the NAE was calculated by averaging the soil moisture estimates from the four GLDAS model versions (i.e., VIC, CLM, Noah, and Mosaic). The associated errors for GLDAS-derived monthly soil moisture estimates were calculated as the mean monthly standard deviation from the four GLDAS model simulations (e.g., Tiwari et al. 2009; Voss et al. 2013; Castle et al. 2014; Joodaki et al. 2014). Errors in soil moisture trends were calculated as the standard deviation of the trends computed from the four GLDAS simulations (Voss et al. 2013; Castle et al. 2014).

2.4 Rainfall Data

Rainfall data were utilized to explore the climatic controls on the temporal variation in TWS_{GRACE} and GWS observed over the NAE. The CMAP data (available at: https://www.esrl.noaa.gov/psd/data/gridded/data.cmap.html) were utilized in this study. CMAP data provide global (88.75°N to 88.75°S) merged precipitation estimates from a variety of satellite- and ground-based sources from January 1979 to January 2017 with spatial and temporal resolutions of 2.5° and one month, respectively (Xie and Arkin 1997). The satellite sources used to produce monthly CMAP data include the Geostationary Operational Environmental Satellite (GOES) Precipitation Index (GPI), the Outgoing Longwave Radiation (OLR)-based Precipitation Index (OPI), the Special Sensor Microwave/Imager (SSM/I), and the microwave sounding unit (MSU). In addition to the aforementioned satellite sources, CMAP also integrates the National Centre for Atmospheric Research (NCAR) reanalysis precipitation data along with the Global Precipitation Climatology Centre

(GPCC) data of ~ 200,000 routinely operating precipitation gauges (Xie and Arkin 1997). Over northern and eastern Africa, it has been demonstrated that CMAP data provide the best spatial and temporal correspondence with gauge-based measurements of rainfall and stream flow (e.g., Adeyewa et al. 2003; Dinku et al. 2008; Beighley et al. 2011; Sylla et al. 2013).

3 Results and Discussion

3.1 Temporal Variations in TWS Anomalies

Figure 2 shows the secular trend images in TWS_{GRACE} estimates generated from CSR spherical harmonics (Fig. 2a), CSR mascon (Fig. 2b), JPL mascon (Fig. 2c), and the average of the three solutions (Fig. 2d) over NAE. Inspection of Fig. 2d indicates that the NAE is experiencing an average negative (− 3 mm/year) TWS_{GRACE} trends during the investigated period. Higher TWS_{GRACE} depletion rates (< − 6 mm/year) are observed over the northeastern parts of NAE. The northern coastal areas as well as the southern parts of the NAE, close to recharge areas in Sudan, are witnessing lower TWS_{GRACE} depletion rates (> − 2 mm/year).

The spatial distributions of negative TWS_{GRACE} trends slightly vary with the source of TWS_{GRACE} data. For example, in case of the CSR mascon solutions (Fig. 2b), areas witnessing a uniform negative (− 3 mm/year) TWS_{GRACE} trend are centered over the NAE; the location of these areas is shifted to the east and to the west in case of CSR spherical harmonics (Fig. 2a) and JPL mascon (Fig. 2c) solutions, respectively. Over the entire NAE, comparison between TWS_{GRACE} trends generated from the three solutions (Fig. 2a-c) with the mean trend (Fig. 2d) indicates that JPL mascon-derived trends (Fig. 2c) are slightly (10%) lower than mean trends (Fig. 2d). However, CSR mascon (Fig. 2b) and spherical harmonics-derived (Fig. 2a) trends explain 96 and 93%, respectively, of the mean trend variabilities (Fig. 2d). This is probably related to the way that the TWS_{GRACE} products have been generated. For example, JPL mascons were generated from 3° spherical caps, UT-CSR mascons were generated from 1° hexagons, and UT-CSR spherical harmonics were smoothed using a 200 km Gaussian filter (spatial resolution: ~ 125,000 km^2).

Figure 3 shows the temporal variations in TWS_{GRACE} time series generated over the NAE. Inspection of Fig. 3 shows an excellent agreement in amplitudes, phases, and trends of TWS_{GRACE} extracted from UT-CSR mascon, JPL mascon, and UT-CSR spherical harmonic solutions. Moreover, the minute observed differences lie mostly within the uncertainty limits of each TWS_{GRACE} estimate. Figure 3 also shows an overall depletion in TWS_{GRACE} estimates extracted from the three different TWS_{GRACE} solutions. Depletion rates of − 3.26 ± 0.16 mm/year (− 2.15 ± 0.11 km^3/year), − 3.73 ± 0.23 mm/year (− 2.46 ± 0.15 km^3/year), and − 3.15 ± 0.30 mm/year (− 2.08 ± 0.20 km^3/year) were observed in TWS_{GRACE} estimates of UT-CSR mascon, JPL mascon, and UT-CSR spherical harmonic solutions, respectively. The average depletion rate over the entire NAE, as calculated from the mean of the three solutions (black line; Fig. 3), is estimated at − 3.38 ± 0.21 mm/year (− 2.23 ± 0.14 km^3/year).

Piecewise trend analysis of the average of the three TWS_{GRACE} solutions (black line; Fig. 3), shown in Table 1, is conducted over four distinctive periods: April 2002 to February 2006 (Period I), March 2006 to March 2008 (Period II), April 2008 to December 2012 (Period III), and January 2013 to June 2016 (Period IV) (black dashed lines;

Table 1 Trends in water budget components averaged over the NAE during the investigated period (April 2002 to June 2016)

Parameter	Unit	Period I 4/2002–2/2006	Period II 3/2006–3/2008	Period III 4/2008–12/2012	Period IV 1/2013–6/2016	Entire time period 4/2002–6/2016
TWS_{GRACE}	mm/year	− 6.40 ± 0.98	*− 0.37 ± 1.14*	− 6.61 ± 0.48	+ 9.38 ± 1.34	− 3.38 ± 0.21
	km^3/year	− 4.23 ± 0.65	*− 0.25 ± 0.75*	− 4.36 ± 0.32	+ 6.19 ± 0.88	− 2.23 ± 0.14
SMS	mm/year	$\underline{-\ 0.83 \pm 0.09}$	− 1.71 ± 0.09	− 1.26 ± 0.03	− 0.62 ± 0.10	− 1.19 ± 0.02
	km^3/year	$\underline{-\ 0.55 \pm 0.06}$	− 1.13 ± 0.06	− 0.83 ± 0.02	− 0.41 ± 0.07	− 0.79 ± 0.01
Lake Nasser	mm/year	− 9.18 ± 0.84	+ 23.79 ± 0.73	− 8.66 ± 0.78	+ 6.19 ± 1.17	*+ 0.42 ± 0.30*
	km^3/year	− 6.06 ± 0.55	+ 15.70 ± 0.48	− 5.72 ± 0.51	+ 4.09 ± 1.43	*+ 0.27 ± 0.20*
Tushka Lakes	mm/year	− 1.56 ± 0.03	− 2.08 ± 0.02	− 3.21 ± 0.05	− 2.26 ± 0.04	− 2.06 ± 0.30
	km^3/year	− 1.03 ± 0.02	− 1.38 ± 0.01	− 2.12 ± 0.03	− 1.49 ± 0.03	− 1.36 ± 0.01
GWS	mm/year	+ 5.16 ± 1.23	− 20.37 ± 1.24	+ 6.52 ± 0.85	+ 6.07 ± 2.54	− 0.55 ± 0.27
	km^3/year	+ 3.41 ± 0.81	− 13.45 ± 0.82	+ 4.31 ± 0.56	+ 4.00 ± 1.68	− 0.36 ± 0.18

Trends that are significant at < 65% level of confidence are underlined, ≥ 65% level of confidence are italic, ≥ 95% level of confidence are normal type face

Fig. 3). Examination of Fig. 3 and Table 1 shows that the NAE is witnessing a TWS_{GRACE} decline during Periods I and III at almost the same rate [Period I: − 6.40 ± 0.98 mm/year (− 4.23 ± 0.65 km^3/year); Period III: −6.61 ± 0.48 mm/year (− 4.36 ± 0.32 km^3/year)] and with a much lower rate during Period II [Period II: − 0.37 ± 1.14 mm/year (− 0.25 ± 0.75 km^3/year)]. However, during Period IV the NAE witnesses a TWS_{GRACE} increase (Period IV: 9.38 ± 1.34 mm/year; 6.19 ± 0.88 km^3/year). The temporal variability in TWS_{GRACE} is related to temporal variations in one or more of the TWS_{GRACE} compartments (e.g., SWS, SMS, and GWS). Below, the temporal variations in each of the TWS_{GRACE} compartments are discussed.

3.2 Temporal Variations in SWS Anomalies

Figure 5a shows the temporal variations in Lake Nasser level anomalies during the examined period. It is worth mentioning that during the investigated period Lake Nasser's maximum height (179.71 m) was observed in November 2007, whereas its minimum height (169.52 m) was observed in July 2012. Lake Nasser general fluctuation is mainly attributed to the seasonality in the Nile River. It has been reported that the Nile River is witnessing 64-, 19-, 12-, and 7-year climate cycles (e.g., Kondrashov et al. 2005). Examination of Fig. 5a shows that Lake Nasser is witnessing an overall height increase of 0.42 ± 0.30 mm/year. Piecewise trend analysis (Table 1) indicates that the Lake Nasser level anomalies are declining (− 9.18 ± 0.84 mm/year) during Period I, increasing (23.79 ± 0.73 mm/year) during Period II, declining (− 8.66 ± 0.78 mm/year) during Period III, and increasing (6.19 ± 1.17 mm/year) during Period IV. Analysis of Lake Nasser trends indicates that the temporal variations in lake levels during Periods I, III, and IV are in phase and consistent with, and largely driving, the temporal variations in TWS_{GRACE}. This assumption is supported by the fact that the TWS_{GRACE} trends, observed during these periods, are correlated with increases and decreases of the level of Lake Nasser during the same periods (Figs. 3 and 5a and Table 1).

The temporal variations in the Tushka Lakes level anomalies are shown in Fig. 5b. Starting in 2002, the Tushka Lakes have witnessed a dramatic decrease in volume, area, and water level. For example, the Tushka Lakes' volumes (areas) are estimated at 27.11 km^3 (1669.62 km^2), 11.81 km^3 (972.42 km^2), 5.55 km^3 (512.72 km^2), and 0.36 km^3 (130.18 km^2) in Januaries of 2002, 2006, 2010, and 2016, respectively. Analysis of temporal variations in the Tushka Lakes' volumes indicates that they cumulatively lost 56, 80, and 98% of their volumes in 2006, 2010, and 2016, respectively, compared to their volume in 2002. The loss in the Tushka Lakes' volumes and areas is believed to be an evaporation loss (e.g., Chipman and Lillesand 2007; Sultan et al. 2013). Examination of Fig. 5b shows that the levels of the Tushka Lakes are experiencing an overall systematic decrease in water levels of − 1.94 ± 0.01 km^3/year that is equivalent to − 1.36 ± 0.01 km^3/year (− 2.06 ± 0.30 mm/year) if distributed over the entire NAE.

3.3 Temporal Variations in SMS Anomalies

Figure 5c shows the temporal variations in GLDAS-derived SMS time series extracted over the NAE. Inspection of Fig. 5c shows that the SMS is witnessing an overall depletion of − 1.19 ± 0.02 mm/year (− 0.79 ± 0.01 km^3/year). Inspection of piecewise trend analysis results (Table 1) and Fig. 5c indicates that the SMS is always declining during the four investigated periods but at varying rates (Period I: − 0.83 ± 0.09 mm/year;

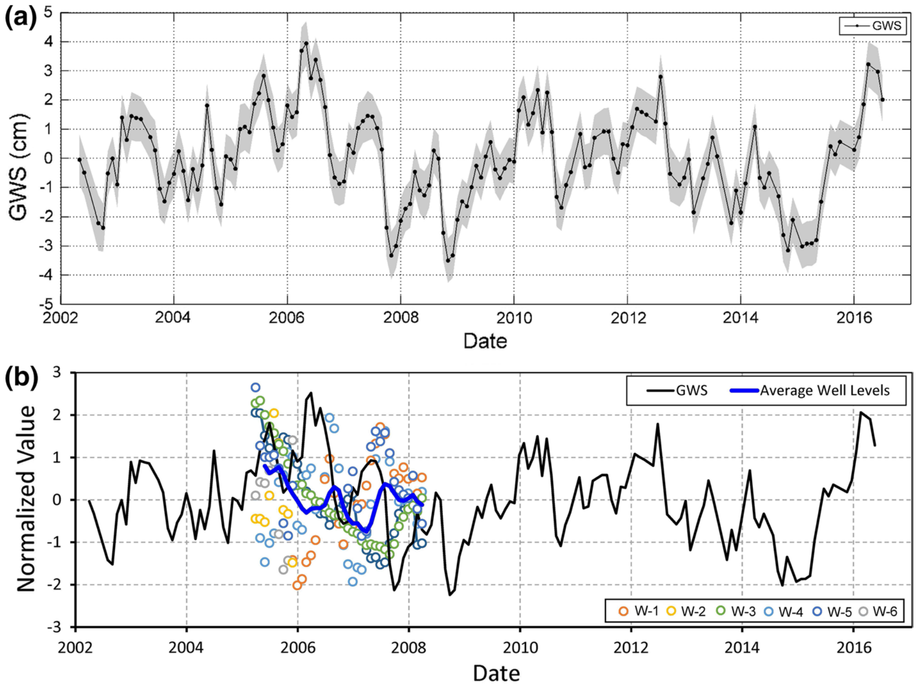

Fig. 6 **a** Temporal variations in the GWS estimates generated over the NAE along with their uncertainty limits. **b** Validation of the GWS anomalies (black solid thick line) against the available monthly well observations (individual well: colored circles; average: blue thick line) over the NAE

Period II: − 1.71 ± 0.09 mm/year; Period III: − 1.26 ± 0.03 mm/year; and Period IV: − 0.62 ± 0.10 mm/year).

3.4 Temporal Variations in GWS Anomalies

Figure 6a shows the GWS time series extracted, according to Eqs. (1) and (2), over the NAE. Inspection of Fig. 6a shows that the NAE is witnessing an overall GWS decline of − 0.55 ± 0.27 mm/year (− 0.36 ± 0.18 km^3/year). Piecewise trend analysis results (Table 1) shows that the NAE is experiencing a GWS increase (5.16 ± 1.23 mm/year; 3.41 ± 0.81 km^3/year) during Period I followed by a sharp GWS decrease (− 20.37 ± 1.24 mm/year; − 13.45 ± 0.82 km^3/year) during Period II, then a GWS increase during periods III and IV (Period III: 6.52 ± 0.85 mm/year, 4.31 ± 0.56 km^3/year; Period IV: 6.07 ± 2.45 mm/year, 4.00 ± 1.68 km^3/year).

Given the paucity of the groundwater-level measurements in the study area, monthly (April 2005 to April 2008) water-level data of six monitoring wells, distributed in the Western Desert of Egypt (refer to Fig. 1 for well locations), were used to validate the GWS variability over the NAE. The water level in these wells ranges from 200.30 m to 246.6 m. Unfortunately, the specific yield information for these wells is not available. Hence, the water-level time series for each well was normalized by its standard deviation following the approach advanced by Castle et al. (2014) where we subtracted the temporal mean from each monthly water-level value and then divided by the temporal standard deviation. The normalized water-level and GRACE-derived GWS measurements are shown in Fig. 6b. Inspection of Fig. 6b indicated that the GRACE-derived GWS estimates generally capture the observed temporal groundwater-level variability during Periods I and II as indicated by the analysis of the available water level data.

3.5 Groundwater Recharge and Depletion Rates and Conditions

Examination of Fig. 6a and Table 1 reveals that the NAE is receiving natural recharge during Periods I (GWS trend: 3.41 ± 0.81 km^3/year), III (GWS trend: 4.31 ± 0.56 km^3/year), and IV (GWS trend: 4.00 ± 1.68 km^3/year). However, the NAE is experiencing GWS depletion of − 13.45 ± 0.82 km^3/year during Period II. The sharp GWS decline rate during Period II is largely related to exceptional drought conditions in Period I compared to the previous periods. Examination of the AAR and Lake Nasser levels indicates a decline during Period I (AAR: 120 mm; Lake Nasser level: 174.6 m) compared to the preceding years (1998–2002; AAR: 133 mm; Lake Nasser level: 178.2 m). Another common contributing factor, for the observed GWS depletion, could be the baseflow recession. Normal baseflow recession occurs naturally during periods of extended drought and could cause extensive water-level declines over time periods of weeks to months that result in volumetrically significant storage depletion (e.g., Alley and Konikow 2015). It is worth mentioning that during Period II the trend of the combined GWS and SWS components still positive (0.88 ± 0.75 km^3/year), suggesting the possible usage of Lake Nasser surface water resources during periods similar to Period II. In other words, during the periods where the GWS trends are declining, Lake Nasser surface water could be used to augment the running irrigation projects and hence minimize the impacts of the GWS decline. One other possible solution could be channeling the encroaching Lake Nasser water, in high flood years such as Period II, across the western plateau reaching the lowlands west of the plateau, that are largely underlain by the Nubian aquifer, to recharge the NAE (e.g., Sultan et al. 2013).

To quantify the recharge rates during Periods I, III, and IV, the discharge rate (natural discharge + anthropogenic groundwater extraction) was added to the GWS trends using the following equation:

$$\text{Recharge} = \Delta\text{GWS} + \text{Discharge}. \tag{3}$$

The sum of the average annual anthropogenic groundwater extraction and the average annual natural discharge for NAE was estimated at 2.85 km^3/year (Sultan et al. 2007; Mohamed et al. 2016). The recharge rates for the NAE are estimated at 6.26 ± 0.81, 7.16 ± 0.56, and 6.85 ± 1.68 km^3/year during Periods I, III, and IV, respectively. The total recharge during Periods I, II, and IV is estimated at 20.27 ± 1.95 km^3; however, approximate average annual recharge rate of 1.66 km^3/year is estimated during the three periods.

The recharge rates of the NAE during Periods I, III, and IV are partially attributed to increasing the AAR during the investigated periods compared to the preceding periods. Comparing AAR approach was used instead of examining the trends in rainfall given the fact that a rainfall value is already a rate and so it corresponds to a trend signal in TWS_{GRACE}, whereas a trend in rainfall corresponds to an increase in TWS_{GRACE} rate. However, a one-to-one correspondence, in magnitudes, is not to be expected, given that AAR could be redistributed as runoff and evapotranspiration that could affect the spatial and temporal distribution of the precipitated water, and hence the recharge locations and magnitudes. Moreover, a progressive shift in timing between the AAR and recharge should be also expected given the time rainfall takes to feed the groundwater in shallow and deep

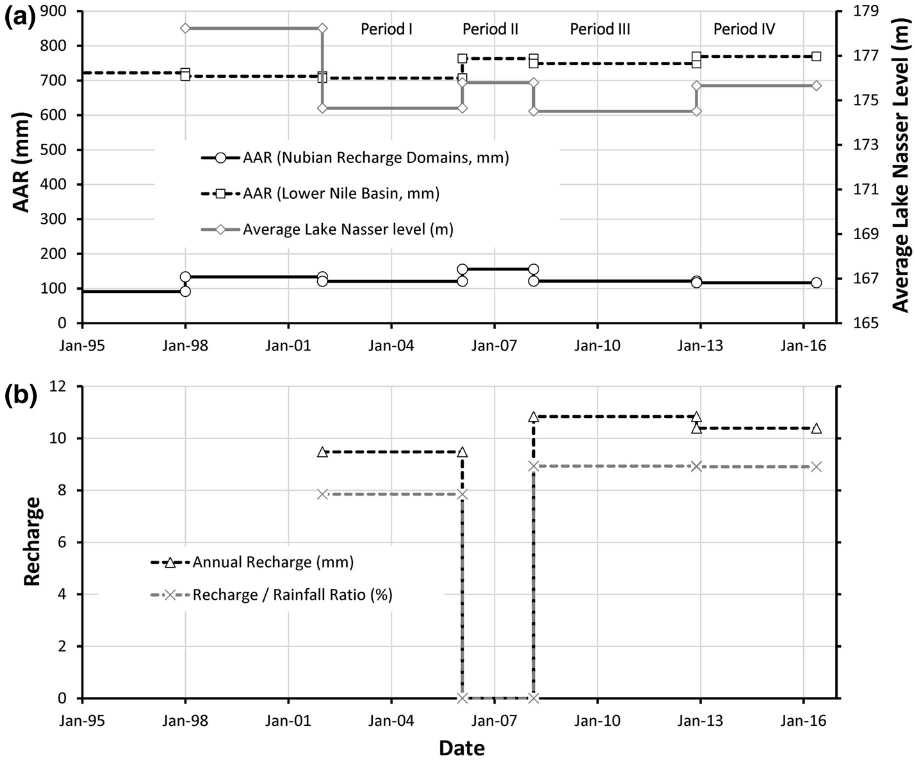

Fig. 7 **a** Temporal variations in AAR generated over the Nubian recharge domains (solid black line) and the lower Nile basin (dashed black line). Average Lake Nasser level (solid gray line) is also shown. **b** Temporal variations in average annual recharge (dashed black line) and recharge-to-rainfall ratio (dashed gray line) over the NAE during the investigated periods

aquifers (e.g., Owor et al. 2009; Ahmed et al. 2011, 2014b; Hocking and Kelly 2016). It is worth mentioning that, over-arid and semiarid regions such as the NAE, only a small portion of any episodic rainfall event will reach the aquifer's water table in the time of this event. However, this portion will increase gradually with time. The time lag between the rainfall and the recharge events depends on magnitude and duration of rainfall, soil type, texture, and hydrologic properties, and density and types of vegetation (e.g., Vogel and Van Urk 1975; Mauth et al. 2003; Döll and Flörke 2005; Keese et al. 2005; Thomas et al. 2016). Over the NAE, for example, the groundwater response to local rainfall events is delayed by 1–4 months; highest rainfall occurs in January; the peak rise in the groundwater level is recorded in April to May (e.g., Sultan et al. 2011; 2013; Gad 2009). These estimates are compared to, and correlated with, those from other arid and semiarid environments of similar geologic and climatic settings (e.g., Döll and Flörke 2005; Thomas et al. 2016; Tirogo et al. 2016). It is worth mentioning that the effective recharge and groundwater flow within the NAE could take thousands of years. For example, a progression of groundwater ages was observed within the NAE from southwest ($< 0.03 \times 10^6$ years) to northeast (1×10^6years). This age progression suggests that the NAE received autochthonous recharge events that were primarily occurred at the foothills of the Uweinat mountainous area (Fig. 1). The spatial distribution of the age progression indicates relatively high groundwater flow velocities (~ 2 m/year) toward the north and low velocities (0.2 m/year) toward the east (e.g., Sturchio et al. 2004; Patterson et al. 2005; Sultan et al. 2013).

Figure 7a shows the AAR for the investigated Periods I, II, III, and IV as well as two preceding periods (1979–1997 and 1998–2002), averaged over the Nubian aquifer outcrops in Chad and Sudan (layout in Fig. 1, inset a) that are receiving AAR greater than 20 mm. A conservative 20 mm/years value was selected based on the fact that, in Egypt a rainfall event of less than 5 mm is not expected to produce a significant recharge and/or runoff events (e.g., Milewski et al. 2009). Examination of Fig. 7a indicates that the AAR over the Nubian aquifer recharge domains increased from 91 mm during 1979–1997 period to 133 during 1998–2002 period. This AAR increase is partially responsible for the groundwater recharge events during Period I. The annual recharge rates as well as the recharge-to-rainfall ratio are displayed in Fig. 7b. Similarly, the increase in the recharge rates during Periods III and IV is related to the increase in the AAR during Periods II and III, respectively. For example, the AAR increased from 120 mm during Period I to 155 mm and 121 mm during Periods II and III, respectively (Fig. 7a, b).

It is worth mentioning that the recharge rates of the NAE during Periods IV are also partially attributed to the increase in Lake Nasser levels. The average Lake Nasser level was estimated at 174.6, 175.7, 174.5, and 175.6 m during Period I, Period II, Period III, and Period IV, respectively. The Lake Nasser level during Period IV is 1.1 m higher than the average level during Period III. The increase in Lake Nasser levels is supported by increasing the AAR over the lower Nile basin (layout in Fig. 1, inset b) during the same periods (Period I: 706 mm; Period II: 763; Period III: 748 mm; and Period IV: 769 mm). The AAR over the lower Nile basin during Period IV is 21 m higher than the AAR during Period III.

Given the current overall GWS depletion rate ($-$ 0.55 $\pm$ 0.27 mm/year; $-$ 0.36 $\pm$ 0.18 km^3/year) during the entire investigated period (April 2002 to June 2016), the longevity of the NAE can be estimated. Based on modeled recoverable groundwater volumes (5180 km^3) (Bakhbakhi 2006), the NAE could last for more than 10,000 years assuming a constant GWS depletion and recharge rates. Increasing depletion rates and/or decreasing the recharge rate would reduce the NAE's longevity.

4 Summary and Conclusions

Egypt is currently seeking additional freshwater resources to pursue its plans for modernization and development. Decision makers are planning to utilize more of Egyptian groundwater resources, at the expenses of the limited Nile River surface water, to support national reclamation projects (1.5×10^6 acre in 5 years). Almost all of the reclamation areas are planned to utilize NAE groundwater resources. The NAE needs to be routinely and continuously monitored because of its importance.

Previous studies that utilized TWS_{GRACE} to monitor the NAE reported groundwater depletion rates varied with the examined period as well as the data sources. In addition, the reported groundwater depletion rates were extracted from the entire time series, ignoring the temporal variability and cyclicity occurred at different time intervals. None of these studies reported groundwater recharge within the NAE. In this study, temporal (April 2002 to June 2016) TWS_{GRACE} data along with the outputs of LSMs were used to provide improved estimates recharge and depletion rates of the NAE and to investigate the interaction of the NAE with the artificial lakes.

Results indicate that during Periods I, III, and IV the NAE is receiving a total recharge of 20.27 ± 1.95 km^3. Recharge events of the NAE occur only under excessive precipitation conditions over the Nubian recharge domains (in Sudan and Chad) and/or under a significant rise in Lake Nasser levels. The sharp GWS decline rate during Period II (− 13.45 ± 0.82 km^3/year) in the NAE is largely related to exceptional drought conditions in Period I compared to the previous periods. Another common contributing factor for the observed GWS depletion could be the normal baseflow recession. However, during this period the trend in the combined GWS and SWS components is still increasing (0.88 ± 0.75 km^3/year) suggesting the possible usage of Lake Nasser surface water resources in development plans.

Findings indicate that Egyptian decision makers are facing a real challenge to provide and maintain sustainable water resource management. However, they are highly recommended to use a conjunctive surface water and groundwater management plan given the fact that in periods where the GWS is declining (e.g., Period II), the SWS of Lake Nasser could be utilized.

The study results demonstrate that global monthly TWS_{GRACE} solutions can provide a practical, informative, and cost-effective approach for monitoring aquifer systems located in any geologic or hydrologic setting across the globe. However, it is worth mentioning that, in the calculations of TWS_{GRACE} and GWS trends, the temporal variations that are related to semiannual, annual, multi-annual, and decadal climatic cycles were assumed to be represented in the examined TWS_{GRACE} record, while the semiannual, annual, and multi-annual cycles are likely to be represented in the available TWS_{GRACE} records, the decadal cycles might not be, given the short GRACE operational period (15 years). The acquisition of TWS_{GRACE} data over the upcoming years by the GRACE-FO (expected in 2017/2018; nominal/expected lifetime: 5/10 years) and GRACE-II (planned in 2025; nominal/expected lifetime: 5/10 years) missions will in part address these limitations by enabling the acquisition of continuous and lengthy TWS_{GRACE} records.

Acknowledgements This work was supported by NASA's Earth Science Division Grant NNX12AJ94G to Western Michigan University. The authors thank the Editor-in-Chief and the anonymous reviewers of the Surveys in Geophysics for their instructive comments and suggestions.

References

A G, Wahr J, Zhong S (2013) Computations of the viscoelastic response of a 3-D compressible Earth to surface loading: an application to Glacial Isostatic Adjustment in Antarctica and Canada. Geophys J Int 192:557–572. https://doi.org/10.1093/gji/ggs030

Adeyewa ZD, Nakamura K (2003) Validation of TRMM radar rainfall data over major Climatic Regions in Africa. J Appl Meteorol 42:331–347. https://doi.org/10.1175/1520-0450(2003)042%3C0331:VOTRRD%3E2.0.CO;2

Ahmed M, Sultan M, Wahr J et al (2011) Integration of GRACE (Gravity Recovery and Climate Experiment) data with traditional data sets for a better understanding of the timedependent water partitioning in African watersheds. Geology 39:479–482. https://doi.org/10.1130/G31812.1

Ahmed M, Sauck W, Sultan M et al (2013) Geophysical Constraints on the hydrogeologic and structural settings of the gulf of suez rift-related basins: case study from the El Qaa Plain, Sinai, Egypt. Surv Geophys 35:415–430. https://doi.org/10.1007/s10712-013-9259-6

Ahmed M, Sultan M, Wahr J et al (2014a) Quantifying recharge and depletion rates of the nubian sandstone aquifer system: an integrated approach. In: GRACE science team meeting (GSTM)

Ahmed M, Sultan M, Wahr J, Yan E (2014b) The use of GRACE data to monitor natural and anthropogenic induced variations in water availability across Africa. Earth Sci Rev 136:289–300. https://doi.org/10.1016/j.earscirev.2014.05.009

Ahmed M, Sultan M, Othman A (2015) Monitoring temporal variations in water resources across the Arabian Peninsula and identification of their controlling factors. In: American Geophysical Union (AGU), Fall Meeting 2015, abstract id. H41F-1396, 2015AGUFM.H41F1396A

Ahmed M, Sultan M, Yan E, Wahr J (2016) Assessing and improving land surface model outputs over Africa using GRACE, field, and remote sensing data. Surv Geophys 37:529–556. https://doi.org/10.1007/s10712-016-9360-8

Alley WM, Konikow LF (2015) Bringing GRACE down to earth. Groundwater 53:826–829. https://doi.org/10.1111/gwat.12379

Al-Zyoud S, Rühaak W, Forootan E, Sass I (2015) Over exploitation of groundwater in the Centre of Amman Zarqa Basin—Jordan: evaluation of well data and GRACE satellite observations. Resources 4:819–830. https://doi.org/10.3390/resources4040819

Bakhbakhi M (2006) Nubian sandstone aquifer system. In: Loucks SF, Crandall DP (eds) Nubian sandstone aquifer system, in non-renewable groundwater resources: a guidebook on socially sustainable management for water-policy makers. United Nations Educational, Scientific and Cultural Org, Paris, pp 75–81

Beighley RE, Ray RL, He Y et al (2011) Comparing satellite derived precipitation datasets using the Hillslope River Routing (HRR) model in the Congo River Basin. Hydrol Process 25:3216–3229. https://doi.org/10.1002/hyp.8045

Birkett CM (1995) The contribution of TOPEX/POSEIDON to the global monitoring of climatically sensitive lakes. J Geophys Res Ocean 100:25179–25204. https://doi.org/10.1029/95JC02125

Castellazzi P, Martel R, Galloway DL et al (2016) Assessing Groundwater depletion and dynamics using GRACE and InSAR: potential and limitations. Groundwater 54:768–780. https://doi.org/10.1111/gwat.12453

Castle S, Thomas B, Reager J et al (2014) Groundwater depletion during drought threatens future water security of the Colorado River Basin. Geophys Res Lett 10:5904–5911. https://doi.org/10.1002/2014GL061055.Received

Cheng M, Ries JC, Tapley BD (2011) Variations of the Earth's figure axis from satellite laser ranging and GRACE. J Geophys Res 116:B01409. https://doi.org/10.1029/2010JB000850

Chinnasamy P, Agoramoorthy G (2015) Groundwater storage and depletion trends in Tamil Nadu State, India. Water Resour Manag 29:2139–2152. https://doi.org/10.1007/s11269-015-0932-z

Chinnasamy P, Sunde MG (2016) Improving spatiotemporal groundwater estimates after natural disasters using remotely sensed data—a case study of the Indian Ocean Tsunami. Earth Sci Informatics 9:101–111. https://doi.org/10.1007/s12145-015-0238-y

Chinnasamy P, Maheshwari B, Prathapar S (2015) Understanding groundwater storage changes and recharge in Rajasthan, India through remote sensing. Water (Switzerland) 7:5547–5565. https://doi.org/10.3390/w7105547

Chipman JW, Lillesand TM (2007) Satellite-based assessment of the dynamics of new lakes in southern Egypt. Int J Remote Sens 28:4365–4379. https://doi.org/10.1080/01431160701241787

Crétaux J-F, Jelinski W, Calmant S et al (2011) SOLS: a lake database to monitor in the Near Real Time water level and storage variations from remote sensing data. Adv Space Res 47:1497–1507. https://doi.org/10.1016/J.ASR.2011.01.004

Dai Y, Zeng X, Dickinson RE et al (2003) The common land model. Bull Am Meteorol Soc 84:1013–1023. https://doi.org/10.1175/BAMS-84-8-1013

Dinku T, Chidzambwa S, Ceccato P et al (2008) Validation of high-resolution satellite rainfall products over complex terrain. Int J Remote Sens 29:4097–4110. https://doi.org/10.1080/01431160701772526

Döll P, Flörke M (2005) Global-scale estimation of diffuse groundwater recharge: model tuning to local data for semi-arid and arid regions and assessment of climate change impact. Frankfurt hydrology paper 3, Institute of Physical Geography, Frankfurt University, Frankfurt am Main, Germany, 26 p

Döll P, Müller Schmied H, Schuh C et al (2014) Global-scale assessment of groundwater depletion and related groundwater abstractions: combining hydrological modeling with information from well observations and GRACE satellites. Water Resour Res 50:5698–5720. https://doi.org/10.1002/2014WR015595

Fallatah OA, Ahmed M, Save H, Akanda AS (2017) Quantifying temporal variations in water resources of a vulnerable middle eastern transboundary aquifer system. Hydrol Process 31:4081–4091. https://doi.org/10.1002/hyp.11285

Feng W, Zhong M, Lemoine J-M et al (2013) Evaluation of groundwater depletion in North China using the Gravity Recovery and Climate Experiment (GRACE) data and ground-based measurements. Water Resour Res 49:2110–2118. https://doi.org/10.1002/wrcr.20192

Gad M (2009) A numerical approach for estimating the monthly groundwater recharge from rainfall, Wadi El-Khour basin, Northwestern coastal zone, Egypt. Egypt J Aquat Res 35:265–280

Gonçalvès J, Petersen J, Deschamps P et al (2013) Quantifying the modern recharge of the “fossil” Sahara aquifers. Geophys Res Lett 40:2673–2678. https://doi.org/10.1002/grl.50478
Hastings WK (1970) Monte Carlo sampling methods using Markov Chains and their applications. Biometrika 57:97. https://doi.org/10.2307/2334940
Hocking M, Kelly BFJ (2016) Groundwater recharge and time lag measurement through Vertosols using impulse response functions. J Hydrol 535:22–35. https://doi.org/10.1016/j.jhydrol.2016.01.042
Huang Z, Pan Y, Gong H et al (2015) Subregional-scale groundwater depletion detected by GRACE for both shallow and deep aquifers in North China Plain. Geophys Res Lett 42:1791–1799. https://doi.org/10.1002/2014GL062498
Huang J, Pavlic G, Rivera A et al (2016) Mapping groundwater storage variations with GRACE: a case study in Alberta, Canada. Hydrogeol J. https://doi.org/10.1007/s10040-016-1412-0
Hulme M, Doherty R, Ngara T et al (2001) African climate change: 1900–2100. Clim Res 17:145–168. https://doi.org/10.3354/cr017145
Huo A, Peng J, Chen X et al (2016) Groundwater storage and depletion trends in the Loess areas of China. Environ Earth Sci 75:1–11. https://doi.org/10.1007/s12665-016-5951-4
Jiang Q, Ferreira VG, Chen J (2016) Monitoring groundwater changes in the Yangtze River basin using satellite and model data. Arab J Geosci. https://doi.org/10.1007/s12517-016-2522-7
Joodaki G, Wahr J, Swenson S (2014) Estimating the human contribution to groundwater depletion in the Middle East, from GRACE data, land surface models, and well observations Gholamreza. Water Resour Res 50:1–14. https://doi.org/10.1002/2013WR014633.Received
Keese KE, Scanlon BR, Reedy RC (2005) Assessing controls on diffuse groundwater recharge using unsaturated flow modeling. Water Resour Res 41:1–12. https://doi.org/10.1029/2004WR003841
Kondrashov D, Feliks Y, Ghil M (2005) Oscillatory modes of extended Nile River records (A.D. 622-1922). Geophys Res Lett 32:1–4. https://doi.org/10.1029/2004GL022156
Koren V, Schaake J, Mitchell K et al (1999) A parameterization of snowpack and frozen ground intended for NCEP weather and climate models. J Geophys Res 104:19569–19585. https://doi.org/10.1029/1999JD900232
Koster RD, Suarez MJ (1996) Energy and water balance calculations in the Mosaic LSM. NASA technical memorandum; 104606. Technical report series on global modeling and data assimilation, vol 9, 60 p.
Lakshmi V (2016) Beyond GRACE: using satellite data for groundwater investigations. Groundwater 54:615–618. https://doi.org/10.1111/gwat.12444
Landerer FW, Swenson SC (2012) Accuracy of scaled GRACE terrestrial water storage estimates. Water Resour Res 48:1–11. https://doi.org/10.1029/2011WR011453
Lenk O (2013) Satellite based estimates of terrestrial water storage variations in Turkey. J Geodyn 67:106–110. https://doi.org/10.1016/j.jog.2012.04.010
Li B, Rodell M (2015) Evaluation of a model-based groundwater drought indicator in the conterminous U.S. J Hydrol 526:78–88. https://doi.org/10.1016/j.jhydrol.2014.09.027
Liang X, Lettenmaier DP, Wood EF (1996) One-dimensional statistical dynamic representation of subgrid spatial variability of precipitation in the two-layer variable infiltration capacity model. J Geophys Res 101:21403. https://doi.org/10.1029/96JD01448
Lillesand TM, Kiefer RW, Chipman JW (2015) Remote sensing and image interpretation. Wiley, New York
Long D, Longuevergne L, Scanlon BR (2015) Global analysis of approaches for deriving total water storage changes from GRACE satellites. Water Resour Res 51:2574–2594. https://doi.org/10.1002/2014WR016853
Long D, Chen X, Scanlon BR et al (2016) Have GRACE satellites overestimated groundwater depletion in the Northwest India Aquifer? Sci Rep 6:24398. https://doi.org/10.1038/srep24398
Luthcke SB, Sabaka TJ, Loomis BD et al (2013) Antarctica, Greenland and Gulf of Alaska land-ice evolution from an iterated GRACE global mascon solution. J Glaciol 59:613–631. https://doi.org/10.3189/2013JoG12J147
Mauth AS, Aliewi A, Kalbouneh A, Messerschmid C (2003) Monthly recharge estimation in Wadi Natuf, Palestine. In: Proceeding of the 2nd international conference on Wadi Hydrology. Amman-Jordan, pp 10–15
Milewski A, Sultan M, Yan E et al (2009) A remote sensing solution for estimating runoff and recharge in arid environments. J Hydrol. https://doi.org/10.1016/j.jhydrol.2009.04.002
Mohamed L, Sultan M, Ahmed M et al (2015) Structural controls on groundwater flow in basement terrains: geophysical, remote sensing, and field investigations in Sinai. Surv Geophys. https://doi.org/10.1007/s10712-015-9331-5
Mohamed A, Sultan M, Ahmed M et al (2016) Aquifer recharge, depletion, and connectivity: inferences from GRACE, land surface models, and geochemical, and geophysical data. GSA Bull. https://doi.org/10.1130/B31460.1

Muala E, Mohamed Y, Duan Z, van der Zaag P (2014) Estimation of reservoir discharges from Lake Nasser and Roseires Reservoir in the Nile Basin Using satellite altimetry and imagery data. Remote Sens 6:7522–7545. https://doi.org/10.3390/rs6087522

Owor M, Taylor RG, Tindimugaya C, Mwesigwa D (2009) Rainfall intensity and groundwater recharge: empirical evidence from the Upper Nile Basin. Environ Res Lett. https://doi.org/10.1088/1748-9326/4/3/035009

Patterson LJ, Sturchio NC, Kennedy BMK et al (2005) Cosmogenic, radiogenic, and stable isotopic constraints on groundwater residence time in the Nubian Aquifer, Western Desert of Egypt. Geochem Geophys Geosystems. https://doi.org/10.1029/2004GC000779

RIGW/IWACO (1988) Hydrogeological mapping of Egypt; scale 1:2,000,000

Rodell M, Houser PR, Jambor U et al (2004) The global land data assimilation system. Bull Am Meteorol Soc 85:381–394. https://doi.org/10.1175/BAMS-85-3-381

Save H, Bettadpur S, Tapley BD (2012) Reducing errors in the GRACE gravity solutions using regularization. J Geod 86:695–711. https://doi.org/10.1007/S00190-012-0548-5

Save H, Bettadpur S, Tapley B (2016) High resolution CSR GRACE RL05 mascons. J Geophys Res 121:7547–7569. https://doi.org/10.1002/2016JB013007

Scanlon BR, Zhang Z, Save H et al (2016) Global evaluation of new GRACE mascon products for hydrologic applications. Water Resour Res 52:9412–9429. https://doi.org/10.1002/2016WR019494

Sefelnasr AM (2007) Development of groundwater low model for water resources management in the development areas of the western desert. Dissertation (Dr. rer. Nat.) Submitted to the Faculty of Natural Sciences III of the Martin-Luther-University Halle-Wittenberg, 190 p.

Sefelnasr A, Gossel W, Wycisk P (2015) Groundwater management options in an arid environment: the Nubian Sandstone Aquifer System, Eastern Sahara. J Arid Environ 122:46–58. https://doi.org/10.1016/j.jaridenv.2015.06.009

Shum C, Yi Y, Cheng K et al (2003) Calibration of JASON-1 altimeter over Lake Erie special issue: Jason-1 calibration/validation. Mar Geod 26:335–354. https://doi.org/10.1080/714044525

Soltan ME, Moalla SMN, Rashed MN, Fawzy EM (2005) Physicochemical characteristics and distribution of some metals in the ecosystem of Lake Nasser, Egypt. Toxicol Environ Chem 87:167–197. https://doi.org/10.1080/02772240500043322

Sturchio NC, Du X, Purtschert R et al (2004) One million year old groundwater in the Sahara revealed by krypton-81 and chlorine-36. Geophys Res Lett. https://doi.org/10.1029/2003gl019234

Sultan M, Yan E, Sturchio N et al (2007) Natural discharge: a key to sustainable utilization of fossil groundwater. J Hydrol 335:25–36. https://doi.org/10.1016/j.jhydrol.2006.10.034

Sultan M, Metwally S, Milewski A et al (2011) Modern recharge to the Nubian Aquifer, Sinai Peninsula: geochemical, geophysical, and modeling constraints. J Hydrol 403:14–24. https://doi.org/10.1016/j.jhydrol.2011.03.036

Sultan M, Ahmed M, Sturchio N et al (2013) Assessment of the vulnerabilities of the Nubian Sandstone Fossil Aquifer, North Africa. In: Pielke RA, Hossain F (eds) Climate vulnerability: understanding and addressing threats to essential resources. Elsevier Inc., Academic Press, New York, pp 311–333

Sultan M, Ahmed M, Wahr J et al (2014a) Monitoring Aquifer depletion from space: Case studies from the Saharan and Arabian Aquifers. In: Lakshmi V (ed) Remote sensing of the terrestrial water cycle. AGU Geophysical Monograph # 206, London, pp 349–366

Sultan M, Ahmed M, Yan E et al (2014b) Management of Egypt's surface and groundwater resources: present and future. In: American Geophysical Union (AGU), Fall Meeting 2014, abstract id. H41E-0883, 2014AGUFM.H41E0883S

Swain A (2011) Challenges for water sharing in the Nile basin: changing geo-politics and changing climate. Hydrol Sci J 56:687–702. https://doi.org/10.1080/02626667.2011.577037

Swenson S, Wahr J (2006) Post-processing removal of correlated errors in GRACE data. Geophys Res Lett 33:L08402. https://doi.org/10.1029/2005GL025285

Swenson S, Wahr J (2009) Monitoring the water balance of Lake Victoria, East Africa, from space. J Hydrol 370:163–176. https://doi.org/10.1016/j.jhydrol.2009.03.008

Swenson S, Chambers D, Wahr J (2008) Estimating geocenter variations from a combination of GRACE and ocean model output. J Geophys Res 113:B08410. https://doi.org/10.1029/2007JB005338

Sylla MB, Giorgi F, Coppola E, Mariotti L (2013) Uncertainties in daily rainfall over Africa: assessment of gridded observation products and evaluation of a regional climate model simulation. Int J Climatol 33:1805–1817. https://doi.org/10.1002/joc.3551

Tapley BD, Bettadpur S, Ries JC et al (2004a) GRACE measurements of mass variability in the Earth system. Science 305(80):503–505. https://doi.org/10.1126/science.1099192

Tapley BD, Bettadpur S, Watkins M, Reigber C (2004b) The gravity recovery and climate experiment: mission overview and early results. Geophys Res Lett 31:1–4. https://doi.org/10.1029/2004GL019920

Thomas B, Behrangi A, Famiglietti J (2016) Precipitation intensity effects on groundwater recharge in the Southwestern United States. Water 8:90. https://doi.org/10.3390/w8030090

Thorweihe U, Heinl M (2002) Groundwater resources of the nubian aquifer system NE-Africa. Observatoire du Sahara et du Sahel, Paris, p 23

Tirogo J, Jost A, Biaou A et al (2016) Climate variability and groundwater response: a case study in Burkina Faso (West Africa). Water 8:171. https://doi.org/10.3390/w8050171

Tiwari VM, Wahr J, Swenson S (2009) Dwindling groundwater resources in northern India, from satellite gravity observations. Geophys Res Lett 36:L18401. https://doi.org/10.1029/2009GL039401

Veit E, Conrad CP (2016) The impact of groundwater depletion on spatial variations in sea level change during the past century. Geophys Res Lett 43:3351–3359. https://doi.org/10.1002/2016GL068118

Velicogna I, Wahr J (2006) Measurements of time-variable gravity show mass loss in Antarctica. Science 311:1754–1756. https://doi.org/10.1126/science.1123785

Vogel J, Van Urk H (1975) Isotopic composition of groundwater in semi-arid regions of southern Africa. J Hydrol 25:23–36. https://doi.org/10.1016/0022-1694(75)90036-0

Vörösmarty CJ, Green P, Salisbury J, Lammers RB (2000) Global water resources: vulnerability from climate change and population growth. Science 289:284–288. https://doi.org/10.1126/science.289.5477.284

Voss KA, Famiglietti JS, Lo M et al (2013) Groundwater depletion in the Middle East from GRACE with implications for transboundary water management in the Tigris-Euphrates-Western Iran region. Water Resour Res 49:904–914. https://doi.org/10.1002/wrcr.20078

Vrugt JA, Vrugt JA, Ter BC et al (2009) Accelerating Markov chain Monte Carlo simulation by differential evolution with self-adaptive randomized subspace sampling. Int J Nonlinear Sci Numer Simul 10:273–290

Wada Y, Lo M-H, Yeh PJ-F et al (2016) Fate of water pumped from underground and contributions to sea-level rise. Nat Clim Change. https://doi.org/10.1038/nclimate3001

Wahr J, Molenaar M, Bryan F (1998) Time variability of the Earth's gravity field: hydrological and oceanic effects and their possible detection using GRACE. J Geophys Res 103:30205–30229. https://doi.org/10.1029/98JB02844

Watkins MM, Wiese DN, Yuan D et al (2015) Improved methods for observing Earth's time variable mass distribution with GRACE using spherical cap mascons. J Geophys Res Solid Earth 120:2648–2671. https://doi.org/10.1002/2014JB011547.Received

Wiese DN, Landerer FW, Watkins MM (2016) Quantifying and reducing leakage errors in the JPL RL05M GRACE mascon solution. Water Resour Res 52:7490–7502. https://doi.org/10.1002/2016WR019344

Wouters B, Bonin JA, Chambers DP et al (2014) GRACE, time-varying gravity, Earth system dynamics and climate change. Rep Prog Phys. https://doi.org/10.1088/0034-4885/77/11/116801

Xie P, Arkin PA (1997) Global precipitation: a 17-year monthly analysis based on gauge observations, satellite estimates, and numerical model outputs. Bull Am Meteorol Soc 78:2539–2558. https://doi.org/10.1175/1520-0477(1997)078%3C2539:GPAYMA%3E2.0.CO;2

Yosri AM, Abd-Elmegeed MA, Hassan AE (2016) Assessing groundwater storage changes in the Nubian aquifer using GRACE data. Arab J Geosci 9:1–9. https://doi.org/10.1007/s12517-016-2593-5